AGU ADVANCING EARTH AND SPACE SCIENCES

Geophysical Research Letters

RESEARCH LETTER
10.1029/2024GL109666

Thermoelastic Properties of Iron-Rich Ringwoodite and the Deep Mantle Aerotherm of Mars

Fei Wang[1,2], Hannah J. Bausch[1], Laura L. Gardner[1], Dongzhou Zhang[3], Katherine Armstrong[2,4], Aaron S. Bell[5], Jiyong Zhao[6], Ercan E. Alp[6], and Steven D. Jacobsen[1]

[1]Department of Earth and Planetary Sciences, Northwestern University, Evanston, IL, USA, [2]Bayerisches Geoinstitut, University of Bayreuth, Bayreuth, Germany, [3]Hawai'i Institute of Geophysics and Planetology, School of Ocean and Earth Science and Technology, University of Hawai'i at Manoa, Honolulu, HI, USA, [4]Advanced Light Source, Lawrence Berkeley National Laboratory, Berkeley, CA, USA, [5]Department of Geological Sciences, University of Colorado, Boulder, CO, USA, [6]Advanced Photon Source, Argonne National Laboratory, Argonne, IL, USA

Abstract The Martian mantle is considered to have a higher Fe/Mg ratio than the Earth's mantle. Ringwoodite, γ-$(Mg,Fe)_2SiO_4$, is likely the dominant polymorph of olivine in the core-mantle boundary (CMB) region of Mars. We synthesized anhydrous iron-rich ringwoodite with molar Mg/(Mg + Fe) = 0.44 and determined its thermal equation of state up to 35 GPa and 750 K by synchrotron X-ray diffraction. Using a third order Birch-Murnaghan equation of state, we obtain K_{T0} = 182 (3) GPa, K′ = 4.6 (2), and α_0 = 3.18 (6) × 10^{-5} K^{-1}. Using these results and an updated mineralogical model with an iron-rich composition of Mg/(Mg + Fe) = 0.75 for the Martian mantle, we estimate ~1900 K for the temperature of the D1000 seismic discontinuity inside Mars. The resulting adiabat predicts a warm aerotherm, which could explain the presence of partial melt at the CMB of Mars recently detected with seismic data from the 2019 InSight mission.

Plain Language Summary Ringwoodite is an abundant silicate mineral inside Earth and Mars, which can incorporate variable amounts of magnesium, iron and water. Mars is thought to be more iron rich and dry compared with Earth, and so Martian ringwoodite is expected to be anhydrous and have elevated Fe/Mg. We synthesized dry, iron-rich ringwoodite at the pressure-temperature conditions of the Martian interior, and then determined its density and compressibility at high temperatures and pressures of the Martian mantle. The results are used to predict the temperature inside Mars by anchoring our measured physical properties to an observed seismic discontinuity at 1,000 km depth. With that, we calculated a temperature curve for inside Mars that may explain why seismic data from the InSight mission show the possibility of partial melt at the base of the Martian mantle.

Key Points:

- Iron has little effect on the thermoelastic properties of anhydrous ringwoodite
- The temperature of the D1000 discontinuity in the mantle of Mars is estimated to be 1,900 K
- An updated mineralogical model for the Martian mantle is presented

Supporting Information:

Supporting Information may be found in the online version of this article.

Correspondence to:

F. Wang and S. D. Jacobsen,
feiwang2020@u.northwestern.edu;
s-jacobsen@northwestern.edu

Citation:

Wang, F., Bausch, H. J., Gardner, L. L., Zhang, D., Armstrong, K., Bell, A. S., et al. (2025). Thermoelastic properties of iron-rich ringwoodite and the deep mantle aerotherm of Mars. *Geophysical Research Letters*, *52*, e2024GL109666. https://doi.org/10.1029/2024GL109666

Received 8 APR 2024
Accepted 4 NOV 2024

Author Contributions:

Conceptualization: Fei Wang, Steven D. Jacobsen
Formal analysis: Fei Wang
Funding acquisition: Steven D. Jacobsen
Investigation: Fei Wang, Hannah J. Bausch, Laura L. Gardner, Dongzhou Zhang, Katherine Armstrong, Aaron S. Bell, Jiyong Zhao, Ercan E. Alp, Steven D. Jacobsen
Methodology: Fei Wang, Hannah J. Bausch, Laura L. Gardner, Steven D. Jacobsen
Supervision: Steven D. Jacobsen
Visualization: Fei Wang, Steven D. Jacobsen

1. Introduction

Ringwoodite is a high-pressure polymorph of olivine, but unlike wadsleyite, forms a complete solid solution between Mg_2SiO_4 and Fe_2SiO_4. Ringwoodite with Mg/(Mg + Fe) = 0.9, that is, $(Mg_{0.9}Fe_{0.1})_2SiO_4$, or Fo90, is considered the dominant phase in the lowermost portion of the Earth's mantle transition zone (e.g., Frost, 2008). Ringwoodite can also store up to 1.2 wt% water in its crystal structure (H. Fei and Katsura, 2020), and has been found hydrous as inclusions in diamond (Pearson et al., 2014). Due to broad interest in the hydration state of Earth's mantle transition zone, the compressibility and elastic-wave velocities of hydrous Fo90 ringwoodite have been extensively studied (e.g., Chang et al., 2015; Mao et al., 2012).

The Martian mantle is conventionally thought to be drier and more iron-rich than Earth's mantle (e.g., Halliday et al., 2001; Shibazaki et al., 2009), leading to a ringwoodite phase with only Fo70–80 (e.g., Bertka & Fei, 1997). Until recently, knowledge of the interior composition of Mars has been deduced mainly from the study of Martian meteorites (e.g., Dreibus & Wanke, 1985), suggesting a molar composition of Mg/(Mg + Fe) = 0.75 for the Martian mantle. The 2019 Mars InSight mission (Lognonné et al., 2019) has expanded possible compositions of the interior of Mars (Lognonné et al., 2023), particularly from the seismic experiment (Khan et al., 2022), which indicated a less iron-rich mantle and more volatile-rich core than previously thought.

The temperature of the interior of Mars, or aerotherm, remains debated, with adiabatic potential temperatures ranging from 1,600 to 1,750 K on the colder side (Durán et al., 2022; Khan et al., 2022) to considerably hotter 1,800–1,900 K (Drilleau et al., 2022). The observed shear wave velocity shows a negative gradient down to

Writing – original draft: Fei Wang, Steven D. Jacobsen
Writing – review & editing: Fei Wang, Hannah J. Bausch, Laura L. Gardner, Dongzhou Zhang, Katherine Armstrong, Aaron S. Bell, Jiyong Zhao, Ercan E. Alp, Steven D. Jacobsen

600 km depth, which may reflect the thermal state in the shallow part of Mars above 600 km depth that cannot be understood in terms of adiabatic temperatures (e.g., Durán et al., 2022). A seismic discontinuity, if associated with a known mineralogical phase transition, could provide a temperature anchor point, as has been constructed for Earth's mantle (e.g., Katsura, 2022; Katsura et al., 2010). The observed shear wave velocity profile reported by Huang et al. (2022) using waveform inversion techniques indicates a seismic discontinuity at around 1,000 km depth (D1000), which is likely the phase transition from olivine to wadsleyite, or directly to ringwoodite.

Calculation of the temperature gradient, especially below D1000, requires P-V-T relationships and heat capacity of the major mantle minerals. Since most thermoelastic studies of ringwoodite have focused on applications to Earth's mantle, they have typically been performed on samples containing only ∼10% iron (e.g., Chang et al., 2015; Jacobsen, 2006; Mao et al., 2012; Nishihara et al., 2004; Ye et al., 2012; Zhou et al., 2022). An accurate P-V-T equation of state (EOS) for Fe-rich ringwoodite would improve the ability to model the temperature profile of the interior of Mars.

Armentrout and Kavner (2011) measured the volume of iron endmember ringwoodite, known as ahrensite, as a function of temperature from 1,400 to 2,200 K, but only at one pressure of ∼11 GPa. Yamanaka (1986) refined the crystal structure of ahrensite at high temperatures, but only at 1 atm and four temperatures up to 1,073 K. Despite such progress in constraining the physical properties of Fe-rich ringwoodite, there remains a need for high data-density and simultaneous pressure-temperature equations of state (EOS) for iron rich compositions to better constrain the composition and properties at deep-mantle conditions of Mars.

We synthesized anhydrous ringwoodite with Fo44 composition at 17 GPa and ∼1,573 K, and performed synchrotron X-ray diffraction (XRD) on it in a resistively heated diamond anvil cell (DAC) up to 30 GPa and 750 K. After combining our new thermoelastic EOS for iron-rich ringwoodite with previous results we modified the thermodynamic database of Holland et al. (2013) accordingly to estimate the temperature of the D1000 discontinuity in the deep mantle of Mars. Adiabats in more iron-rich and less iron-rich compositional models were used to estimate the temperatures in the core-mantle boundary (CMB) region, which could be nearly high enough in an iron-rich mantle to produce the partial melting at the CMB that is observed by the recent InSight mission seismic experiment (Khan et al., 2023; Samuel et al., 2023).

2. Materials and Methods

Synthesis was carried out in run Z1857 of the 5,000 ton multi-anvil press at Bayerisches Geoinstitut, Germany. Powders of Fe_2O_3, SiO_2 and MgO were dried at 1,273 K before weighing in proportions to produce a Fo44 + En83 composition. Pellets of the mixture were reduced at 1373 K for 24 hr in a CO-CO_2 gas mixing furnace 2 log units below the fayalite-magnetite-quartz (FMQ) buffer. The starting material was loaded, without the addition of water, into a Pt capsule and compressed in a 18/8 assembly with a stepped $LaCrO_3$ furnace. Heating was initiated at 17 GPa and raised at 100 K/min until reaching 1773 K maximum temperature for about one minute before cooling at about 25 K/min to reach 1373 K and holding for 3 hr before quenching. The run product consisted of dark-colored, almost black ringwoodite, and light-blue colored enstatite, in roughly equal proportions (Figure S1 in Supporting Information S1).

Compositional analyses were conducted on a JEOL 8230 electron microprobe at the University of Colorado, Boulder. The electron microprobe analyses (EMPA) were performed using a beam energy of 15 keV, 20 nA beam current and a beam diameter of 2 μm. EMPA data and the analyses of standards from Astimex LTD are provided in Table S1 in Supporting Information S1. The average value of Mg/(Mg + Fe) from 11 points measured over two crystals is 0.442 (5).

Synchrotron Mössbauer spectroscopy (SMS) data were collected using 153 ns pulses of synchrotron radiation on beamline 3-ID-B of the Advanced Photon Source (APS), Argonne National Laboratory. An energy bandwidth of 1 meV was achieved at 14.4125 keV using a silicon double crystal monochromator and 4-bounce in-line high resolution monochromator (Toellner, 2000). Nuclear delay signals were recorded in the 21–128 ns time window of each pulse and curve-fitted using CONUSS 2.2.0 (Sturhahn, 2000) (Figure S2; Table S2 in Supporting Information S1). A two-doublet model with one doublet each for octahedral Fe^{2+} and Fe^{3+} produced the best fit. Hyperfine parameters are provided in Table S3 in Supporting Information S1. Results indicate that the ringwoodite contains 13.1 (2)% Fe^{3+}.

Raman spectra were collected using a 458 nm excitation laser, focused to ~1 μm spot size through a 100x objective (NA = 0.4). Using power above 1 mW at the focal point caused damage to the very dark ringwoodite crystals, so the power was reduced to 0.8 mW and spectra were collected using a 1,200 lines/mm grating, 0.3 m spectrograph and Newton DU970 EMCCD camera from Andor Technology Ltd. Collection times of 30–60 s were averaged over 5–6 accumulations. Raman spectra of the ringwoodite and co-existing enstatite from run Z1857 are shown in Figures S3–S10 in Supporting Information S1, and spectra are provided in Tables S4–S6 in Supporting Information S1.

Compression data at 300 K were obtained in a short-symmetric diamond anvil cell (DAC) using 300 μm Boehler-Almax anvils and seats with ~80° opening (±40° 2θ). A single-crystal polished to ~10 μm thickness was used for the diffraction experiments, loaded together with a ruby pressure calibrant. High-temperature compression data were obtained using an externally heated BX90-type DAC equipped with 300 μm flat culets, gold foil as the pressure calibrant, and single-crystal samples. The heater was made from 0.33 m of 0.2 mm annealed Pt wire, wound through 18 holes of an alumina holder to produce a resistance of ~1 Ω at 300 K. All high-pressure experiments were conducted using a neon pressure transmitting medium, loaded using the COMPRES-GSECARS system (Rivers et al., 2008). Temperatures were determined by a K type thermocouple attached to one of the diamond anvils. With the thermocouple placed in contact with one of the diamond anvils, the temperature uncertainty is estimated to be ±10 K at our highest temperature of 750 K (Zhou et al., 2022). At 300 K we used the ruby pressure calibration of Dewaele et al. (2004). At high temperatures we used the gold pressure scale from Fei et al. (2007). Compression data are provided in Table S7 in Supporting Information S1.

XRD data were collected on beamline 13-BM-C of the APS. The incident X-ray beam was monochromatized to 0.434 Å wavelength and focused into a 15 × 15 μm^2 spot. A Pilatus 1M detector with a 1 mm thick silicon sensor was used to collect the diffraction intensities (Zhang et al., 2017). An integrated area diffraction data set at ambient conditions is provided in Table S8 in Supporting Information S1. Intensity data for crystal structure refinement at ambient conditions was collected prior to gas loading with neon (.cif file provided in SM). High-pressure data at 300 K were collected in ~1.5 GPa pressure steps. Indexing and processing of the diffraction data to obtain unit-cell parameters was carried out using the APEX3 software from Bruker. For the high pressure and high temperature diffraction patterns, integration was performed using the Dioptas software (Prescher & Prakapenka, 2015). The diffraction peaks were fitted using Gaussian functions, which were then used to derive the lattice parameters using the UnitCell software (T. Holland and Redfern, 1997).

3. Results

3.1. Sample Characterization

Raman spectra of three random ringwoodite crystals from the capsule are shown in Figure S3 in Supporting Information S1. In addition to the characteristic doublet at about 796 and 839 cm^{-1}, there is an unknown peak at 675 cm^{-1} not associated with ringwoodite or wadsleyite. Attempts to obtain FTIR spectra were unsuccessful due to the lack of signal through the crystals, which were too dark for us to see any visible light transmission, even when polished to ~10 μm or less. To constrain the possible hydration state of the ringwoodite, we collected Raman spectra of a hydrous Fo87 sample from run Z0140 of Smyth et al. (2003) containing ~1.0 wt% H_2O using the same collection parameters (Figures S4 and S5 in Supporting Information S1). Although a clear OH stretching band is observed in the hydrous sample Z0104 well above a linear baseline drawn between 2,500 and 4,000 cm^{-1}, the same baseline plotted below the spectrum of sample Z1857 shows no detectable sign of water (Figure S6 in Supporting Information S1). In addition, the structure refinement showed no cation vacancies at the octahedral or tetrahedral sites, further evidence that the sample is nominally anhydrous (Ganskow et al., 2010). Therefore, we treat the composition of ringwoodite as anhydrous. Combining Mg/(Mg + Fe) = 0.442 (5) with Si number close to 1 from EMPA, $Fe^{3+}/\Sigma Fe$ = 0.13 (2) from SMS and achieving charge balance results in the approximate formula, $(Mg^{2+}_{0.428}Fe^{2+}_{0.467}Fe^{3+}_{0.070})_2SiO_4$.

3.2. Equation of State at 300 K

The unit cell volumes of Fo44 ringwoodite at high pressures are given in Table S7 in Supporting Information S1. We performed three separate runs and combined all the 300 K data to fit Birch-Murnaghan equation of state (BM-EOS) parameters using EoSFit7 (Angel et al., 2014; Gonzalez-Platas et al., 2016). The resulting EOS parameters

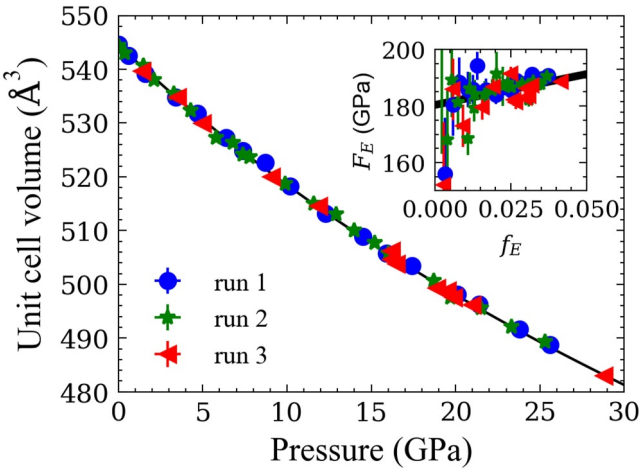

Figure 1. Compression data at 300 K for anhydrous Fo44 ringwoodite from this study across three runs, indicated by three different colors. The solid curve is the third-order BM-EOS fitted to all the data. The inset shows normalized stress (F_E) versus Eulerian strain (f_E) and the statistical significance of K′>4 for iron-rich ringwoodite.

are $V_0 = 544.0\ (2)$ Å^3, $K_{T0} = 189.7\ (9)$ with K′ = 4 (fixed) for the second order BM-EOS, and $V_0 = 544.4\ (2)$ Å^3, $K_{T0} = 182\ (3)$ with K′ = 4.6 (2) for the third order BM-EOS. The pressure-volume data are shown in Figure 1 together with the third order BM-EOS, which is fit to the combined data from the three runs. A plot of normalized stress, $F_E = P/3f_E(1 + 2f_E)^{5/2}$, versus Eulerian strain, $f_E = \left((V_0/V)^{2/3} - 1\right)/2$, is shown inset in Figure 1 to allow visual inspection of the quality of the EOS fit. The straight line fitted from all the F_E–f_E data indicates a statistically significant positive slope, indicating a K′ value higher than 4, consistent with our third order BM-EOS parameters.

3.3. Thermal Equation of State

Having established a reliable isothermal EOS for dry Fo44 at 300 K, we used a high-temperature BM-EOS to fit all the XRD data up to 28 GPa and 750 K using EoSFit7 (Angel et al., 2014; Gonzalez-Platas et al., 2016). With V_{T0}, K_{T0} and K'_{T0} fixed from the isothermal EOS, the resulting coefficient of thermal expansion is $\alpha_0 = 3.3\ (2) \times 10^{-5}$ K^{-1} and $(\partial K_T/\partial T)_P = -0.021\ (6)$ GPa/K. Holding $(\partial K_T/\partial T)_P$ constant while allowing α to vary with pressure leads to non-physical values of α at higher pressures (Helffrich and Connolly, 2009). Therefore, we also applied a Tait thermal EOS modified by T. Holland and Powell (2011), which uses the Einstein function to represent thermal pressure. Using this approach, we estimate an Einstein temperature θ_E of ~425 K, from which we obtain $\alpha_0 = 3.18\ (6) \times 10^{-5}$ K^{-1}. We note that uncertainty in the estimated θ_E does not strongly impact the fitted value of the thermal expansion coefficient (Angel et al., 2014), for example, if θ_E has an uncertainty of ±100 K, the fitted thermal expansion coefficient has the same value of 3.18×10^{-5} K^{-1} with resulting uncertainty of $\pm 0.20 \times 10^{-5}$ K^{-1}. The pressure-temperature-volume data are shown in Figure 2, along with the thermal equation of state.

3.4. Effect of Iron in Ringwoodite

A summary of equation of state parameters for ringwoodite from previous studies is provided in Table S9 in Supporting Information S1. The bulk modulus of anhydrous ringwoodite is expected to increase with Fe content across the solid solution by an amount bX_{Fe}, where X_{Fe} = Fe/(Mg + Fe) and b is the slope of a linear curve for K versus X_{Fe}. Published values of b = 15 (Weidner et al., 1984), 36 (Sinogeikin et al., 1998), 16 (Higo et al., 2006), 18.1 (Liu et al., 2008) and 7.0 (1) (Liu et al., 2016) overpredict our determined value of K_T for Fo44 by 6–18 GPa, or 3–10%, which is far outside our calculated uncertainty. Our determined bulk modulus of 182 (2) GPa is identical within error or even slightly lower than expected for Mg endmember ringwoodite with K = 182–185 GPa (Higo et al., 2006; Li, 2003) only 2 GPa lower than K_T of ahrensite (Nestola et al., 2010), indicating that Mg/Fe substitution in ringwoodite does not significantly change the bulk modulus. We used K_T = 187 (GPa) for the bulk modulus for ahrensite (Figure S10 in Supporting Information S1).

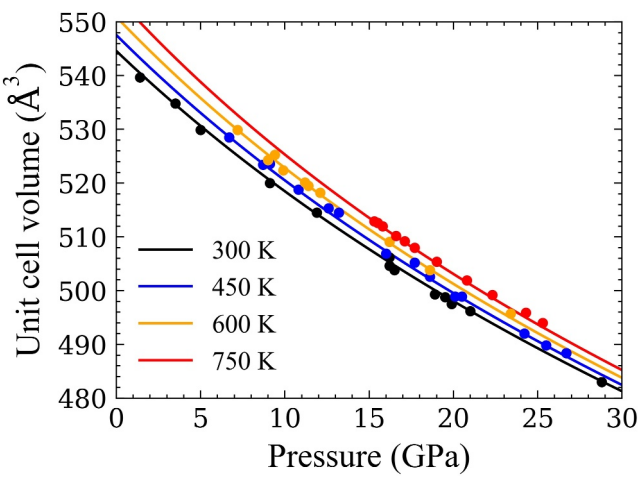

Figure 2. High-temperature compression data for anhydrous Fo44 ringwoodite. Solid curves represent isothermal compression at 300, 450, 600 and 750 K calculated using the EOS from T. Holland and Powell (2011). Data points shown are from the high temperature BX90 run. For clarity, the complete set of 300 K data appear in Figure 1.

The correlation between the bulk modulus and its first pressure derivative is close to one (e.g., Angel, 2014). Therefore, to gain a better understanding of the effects of iron on K and K′, we compiled data from previous studies that reported error in both K and K′ and filtered for results with compression above 10 GPa. By correlating these data, shown in Figure S10 in Supporting Information S1, the result indicates that iron does not significantly change the bulk modulus, but it likely increases K′. The result also shows the strong increase in volume with Fe content (Ganskow et al., 2010; Liu et al., 2016).

The thermal expansion coefficient of ringwoodite obtained in this study is slightly higher than $2.59–3.07 \times 10^{-5}$ K^{-1} for the Mg endmember (Inoue

et al., 2004; Katsura et al., 2004) and 2.7 (3) × 10^{-5} K^{-1} (Yamanaka, 1986) for ahrensite. Since hydrous ringwoodite is known to have a smaller thermal expansion coefficient (Inoue et al., 2004; Ye et al., 2012), the very low implied value of 1.75 × 10^{-5} K^{-1} for ahrensite measured by Armentrout and Kavner (2011) may be attributable to hydration. Taking all studies into account, we do not report a significant change in α_0 with increasing Fe content.

4. Discussion

We developed a mineralogical model for the mantle of Mars with these results and other recent additions to the equations of state database to evaluate the recently measured seismic profile of the interior of Mars. We used the thermodynamic database of Holland et al. (2013) but made the following modifications: (a) We used our deduced values for the thermoelastic properties of ahrensite from Section 3.4. Because those used in the database, sourced from earlier studies, deviate significantly from what is expected by trends presented in this paper. (b) We shifted the olivine-ahrensite loop toward the Mg-rich side to be consistent with the results of Chanyshev et al. (2021). We only modified the thermal expansion coefficient and temperature derivatives of the elastic properties of ahrensite and the interaction parameters between the Mg and Fe endmembers of ringwoodite and wadsleyite. To make adjustments to the phase boundary, we manually changed the interaction parameters until the phase boundary fit the experimental data, shown in Figure S11 in Supporting Information S1. To double-check the accuracy of our thermodynamic model, we calculated a phase diagram using the composition of Bertka and Fei (1997) and compared it with their experimental results. This is shown in Figure S12 in Supporting Information S1, which demonstrates a good fit between our model and their data. Using the modified database, two mineralogical models for the mantle of Mars were constructed from bulk compositional models wherein one is relatively Mg-rich (Fo80) from Khan et al. (2022) and one is more Fe-rich (Fo75) from Taylor (2013). The phase diagrams as well as entropy were computed using Perple_X (Connolly, 2005, 2009) with the thermodynamic parameters described in the text. The resulting phase diagrams are shown in Figure 3, and the calculation of how the phase diagram varies in the MgO-FeO-SiO_2 system with iron content and temperature is shown in Figure S13 in Supporting Information S1.

Huang et al. (2022) found a seismic discontinuity at around 1,000 km depth (D1000), which is believed to represent a phase transition from olivine to its high-pressure polymorph. First, we estimated the temperature at D1000 in Mars with the same method used by Katsura et al. (2010, 2022), who estimated the temperature of the 410-km discontinuity in Earth using the olivine to wadsleyite transition. For D1000, we obtain ~1,700 K in the lower Fe model and ~1900 K in the higher Fe model. Using these temperatures and including all the mantle minerals, we calculated a self-consistent adiabatic temperature profile for each model (Figure 3), where by self-consistency, we mean that at each depth, the temperature was adjusted to make the entropy of the rock the same as at D1000. Phase equilibria data along the temperature profiles were used to calculate the corresponding bulk sound speed profiles for the two Martian mantle composition models. We then made a comparison with the D1000 feature detected by Huang et al. (2022) of a rather sharp discontinuity having a pressure interval of 0.76 (51) GPa. This depth interval is in good agreement with the mineralogical models we calculated for both compositions, which show a discontinuity interval of 0.8 GPa. However, to match the D1000 feature, the temperature at D1000 in the more iron-rich model is very high, ~1,900 (50) K, compared to the lower Fe model of ~1,700 (50) K. Consequently, the CMB region of the iron-rich model would be near 2000 K. Although still lower than the solidus of ~2,400 K (Duncan et al., 2018), if even minor amounts of volatiles are present near the CMB of Mars such as H, K, Na or P, the solidus could be depressed by a few hundred degrees (e.g., Hirschmann, 2000). Based in part on our equations of state for Fe-rich ringwoodite and the new mineralogical models, we predict that a more Fe-rich Martian mantle with some volatiles would be close to or above the requirements for partial melting at the CMB, which can explain the partial melt layer recently observed in the seismic data from Mars (Khan et al., 2023; Samuel et al., 2023).

5. Conclusions

Iron has little effect on the thermoelastic properties of ringwoodite, at least up to relatively high temperatures (750 K) achieved in this study at pressures of the CMB of Mars. Using the results of this study to produce mineralogical models for a somewhat iron-rich Martian mantle, along with the observed depth interval of the

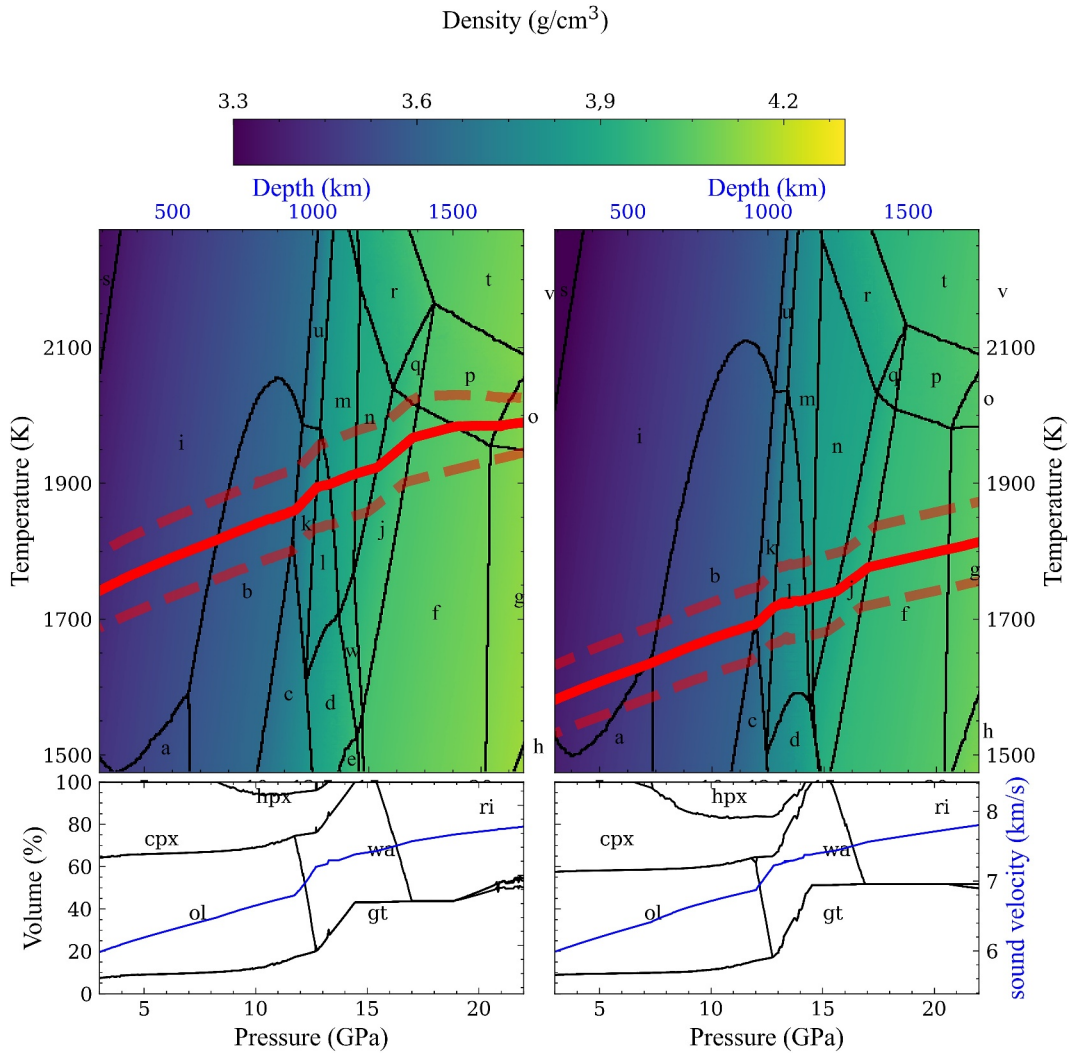

Figure 3. Phase diagrams calculated using the new equation of state for ringwoodite in two different compositional models of Mars, with Fo75 (Taylor et al., 2013) at left, and Fo80 (Kahn et al., 2022) at right. The density is shown by the color scale. The solid red lines represent adiabatic temperature profiles with ±50 K uncertainty (dashed lines) giving the best fit to our estimated ~1900 K temperature at the D1000 discontinuity in the mantle of Mars. Phase proportions in percent volume versus pressure are shown along the bottom with bulk sound speed profiles (blue lines) along the respective adiabats. (a) clinopyroxene (Cpx) + olivine (Ol) + orthopyroxene (Opx) + garnet (Gt); (b) Cpx + Ol + Gt + high-P polymorph (HPx); (c) Cpx + Ol + Gt + ringwoodite (Ri) + Hpx; (d) Cpx + Gt + Hpx + Ri + wadsleyite (Wad); (e) Cpx + Gt + Hpx + Ri; (f) Gt + Ri; (g) Gt + Ri + CaSi^perovskite (Cpv); (h) Gt + Ri + Cpv + akimotoite (Aki); (i) Cpx + Ol + Gt; (j) Gt + Ri + Wad; (k) Cpx + Ol + Gt + Hpx + Wad; l: Cpx + Gt + Hpx + Wad; m: Cpx + Gt + Wad; n: Gt + Wad; o: Gt + Ri + Cpv + ferropericlase (Fp); p: Ri + Fp; q: Gt + Wad + Fp; r: Gt + Wad + Fp; s: Cpx + Ol; t: Gr + Fp; u: Cpx + Ol + Gt + Wad; u: Cpx + Ol + Gt + Wad; v: Gt + Cpv + Fp; w: Cpx + Gt + Ri + Wad.

D1000 discontinuity obtained from the InSight mission, we conclude that a more iron-rich mantle than that of Khan et al. (2022) and/or volatiles are required to explain the presence of partial melt at the base of the mantle of Mars.

Data Availability Statement

Data supporting the findings of this study as well as the thermodynamics data file used to calculate Figure 3 and Figure S11 in Supporting Information S1 are available at Wang (2024). Software: Perple_X version 6.8.8 used for thermodynamic modeling is available for download from: https://perplex.ethz.ch/perplex/ibm_and_mac_archives/WINDOWS/previous_version/.

Acknowledgments
This research was supported by the Alexander von Humboldt Foundation, the US National Science Foundation (NSF) award EAR-1853521, and the Chicago/DOE Alliance Center (CDAC) to SDJ. Work performed at GeoSoilEnviroCARS (The University of Chicago, Sector 13), Advanced Photon Source (APS), Argonne National Laboratory. GeoSoilEnviroCARS is supported by the National Science Foundation—Earth Sciences (EAR-1634415) and Department of Energy—GeoSciences (DE-FG02-94ER14466). This research used resources of the Advanced Photon Source, a U.S. Department of Energy (DOE) Office of Science User Facility operated for the DOE Office of Science by Argonne National Laboratory under Contract No. DE-AC02-06CH11357. Use of the COMPRES-GSECARS gas loading system was supported by COMPRES under NSF Cooperative Agreement EAR—1661511. Single-crystal diffraction experiments on beamline 13-BM-C were supported in part by the Partnership for Extreme Crystallography (PX^2) under NSF EAR-1661511. We thank Sergey Tkachev for help with gas loading. We thank Hongzhan Fei and two anonymous reviewers for their useful suggestions.

References

Angel, R. J., Alvaro, M., & Gonzalez-Platas, J. (2014). EosFit7c and a Fortran module (library) for equation of state calculations. *Zeitschrift für Kristallographie - Crystalline Materials*, *229*(5), 405–419. https://doi.org/10.1515/zkri-2013-1711

Armentrout, M., & Kavner, A. (2011). High pressure, high temperature equation of state for Fe_2SiO_4 ringwoodite and implications for the Earth's transition zone. *Geophysical Research Letters*, *38*(8). https://doi.org/10.1029/2011GL046949

Bertka, C. M., & Fei, Y. (1997). Mineralogy of the Martian interior up to core-mantle boundary pressures. *Journal of Geophysical Research*, *102*(B3), 5251–5264. https://doi.org/10.1029/96JB03270

Chang, Y. Y., Jacobsen, S. D., Bina, C. R., Thomas, S. M., Smyth, J. R., Frost, D. J., et al. (2015). Comparative compressibility of hydrous wadsleyite and ringwoodite: Effect of H2O and implications for detecting water in the transition zone. *Journal of Geophysical Research: Solid Earth*, *120*(12), 8259–8280. https://doi.org/10.1002/2015JB012123

Chanyshev, A., Bondar, D., Fei, H., Purevjav, N., Ishii, T., Nishida, K., et al. (2021). Determination of phase relations of the olivine–ahrensite transition in the Mg_2SiO_4–Fe_2SiO_4 system at 1740 K using modern multi-anvil techniques. *Contributions to Mineralogy and Petrology*, *176*, 1–10. https://doi.org/10.1007/s00410-021-01829-x

Connolly, J. A. D. (2005). Computation of phase equilibria by linear programming: A tool for geodynamic modeling and its application to subduction zone decarbonation. *Earth and Planetary Science Letters*, *236*(1–2), 524–541. https://doi.org/10.1016/j.epsl.2005.04.033

Connolly, J. A. D. (2009). The geodynamic equation of state: What and how. *Geochemistry, Geophysics, Geosystems*, *10*(10). https://doi.org/10.1029/2009GC002540

Dewaele, A., Loubeyre, P., & Mezouar, M. (2004). Equations of state of six metals above 94 GPa. *Physical Review B*, *70*(9), 094112. https://doi.org/10.1103/PhysRevB.70.094112

Dreibus, G., & Wanke, H. (1985). Mars, a volatile-rich planet. *Meteoritics*, *20*(2), 367–381. (ISSN 0026-1114).

Drilleau, M., Samuel, H., Garcia, R. F., Rivoldini, A., Perrin, C., Michaut, C., et al. (2022). Marsquake locations and 1-D seismic models for Mars from InSight data. *Journal of Geophysical Research: Planets*, *127*(9), e2021JE007067. https://doi.org/10.1029/2021JE007067

Duncan, M. S., Schmerr, N. C., Bertka, C. M., & Fei, Y. (2018). Extending the solidus for a model iron-rich Martian mantle composition to 25 GPa. *Geophysical Research Letters*, *45*(19), 10–211. https://doi.org/10.1029/2018GL078182

Durán, C., Khan, A., Ceylan, S., Charalambous, C., Kim, D., Drilleau, M., et al. (2022). Observation of a core-diffracted P-wave from a farside impact with implications for the lower-mantle structure of Mars. *Geophysical Research Letters*, *49*(21), e2022GL100887. https://doi.org/10.1029/2022GL100887

Fei, H., & Katsura, T. (2020). High water solubility of ringwoodite at mantle transition zone temperature. *Earth and Planetary Science Letters*, *531*, 115987. https://doi.org/10.1016/j.epsl.2019.115987

Fei, Y., Ricolleau, A., Frank, M., Mibe, K., Shen, G., & Prakapenka, V. (2007). Toward an internally consistent pressure scale. *Proceedings of the National Academy of Sciences*, *104*(22), 9182–9186. https://doi.org/10.1073/pnas.0609013104

Frost, D. J. (2003). The structure and sharpness of (Mg, Fe) $_2SiO_4$ phase transformations in the transition zone. *Earth and Planetary Science Letters*, *216*(3), 313–328. https://doi.org/10.1016/S0012-821X(03)00533-8

Frost, D. J. (2008). The upper mantle and transition zone. *Elements*, *4*(3), 171–176. https://doi.org/10.2113/GSELEMENTS.4.3.171

Ganskow, G., Ballaran, T. B., & Langenhorst, F. (2010). Effect of iron on the compressibility of hydrous ringwoodite. *American Mineralogist*, *95*(5–6), 747–753. https://doi.org/10.2138/am.2010.3420

Gonzalez-Platas, J., Alvaro, M., Nestola, F., & Angel, R. (2016). EosFit7-GUI: A new graphical user interface for equation of state calculations, analyses and teaching. *Journal of Applied Crystallography*, *49*(4), 1377–1382. https://doi.org/10.1107/S1600576716008050

Halliday, A. N., Wänke, H., Birck, J. L., & Clayton, R. N. (2001). The accretion, composition and early differentiation of Mars. *Space Science Reviews*, *96*(1/4), 197–230. https://doi.org/10.1023/A:1011997206080

Helffrich, G., & Connolly, J. A. D. (2009). Physical contradictions and remedies using simple polythermal equations of state. *American Mineralogist*, *94*(11–12), 1616–1619. https://doi.org/10.2138/am.2009.3262

Higo, Y., Inoue, T., Li, B., Irifune, T., & Liebermann, R. C. (2006). The effect of iron on the elastic properties of ringwoodite at high pressure. *Physics of the Earth and Planetary Interiors*, *159*(3–4), 276–285. https://doi.org/10.1016/j.pepi.2006.08.004

Hirschmann, M. M. (2000). Mantle solidus: Experimental constraints and the effects of peridotite composition. *Geochemistry, Geophysics, Geosystems*, *1*(10). https://doi.org/10.1029/2000GC000070

Holland, T. J., Hudson, N. F., Powell, R., & Harte, B. (2013). New thermodynamic models and calculated phase equilibria in NCFMAS for basic and ultrabasic compositions through the transition zone into the uppermost lower mantle. *Journal of Petrology*, *54*(9), 1901–1920. https://doi.org/10.1093/petrology/egt035

Holland, T. J. B., & Powell, R. (2011). An improved and extended internally consistent thermodynamic dataset for phases of petrological interest, involving a new equation of state for solids. *Journal of Metamorphic Geology*, *29*(3), 333–383. https://doi.org/10.1111/j.1525-1314.1998.00140.x

Holland, T. J. B., & Redfern, S. A. T. (1997). Unit cell refinement from powder diffraction data; the use of regression diagnostics. *Mineralogical Magazine*, *61*(1), 65–77. https://doi.org/10.1180/minmag.1997.061.404.07

Huang, Q., Schmerr, N. C., King, S. D., Kim, D., Rivoldini, A., Plesa, A. C., et al. (2022). Seismic detection of a deep mantle discontinuity within Mars by InSight. *Proceedings of the National Academy of Sciences*, *119*(42), e2204474119. https://doi.org/10.1073/pnas.22044741

Inoue, T., Tanimoto, Y., Irifune, T., Suzuki, T., Fukui, H., & Ohtaka, O. (2004). Thermal expansion of wadsleyite, ringwoodite, hydrous wadsleyite and hydrous ringwoodite. *Physics of the Earth and Planetary Interiors*, *143*, 279–290. https://doi.org/10.1016/j.pepi.2003.07.021

Jacobsen, S. D. (2006). Effect of water on the equation of state of nominally anhydrous minerals. *Reviews in Mineralogy and Geochemistry*, *62*(1), 321–342. https://doi.org/10.2138/rmg.2006.62.14

Katsura, T. (2022). A revised adiabatic temperature profile for the mantle. *Journal of Geophysical Research: Solid Earth*, *127*(2), e2021JB023562. https://doi.org/10.1029/2021JB023562

Katsura, T., Yokoshi, S., Song, M., Kawabe, K., Tsujimura, T., Kubo, A., et al. (2004). Thermal expansion of Mg_2SiO_4 ringwoodite at high pressures. *Journal of Geophysical Research*, *109*(B12). https://doi.org/10.1029/2004JB003094

Katsura, T., Yoneda, A., Yamazaki, D., Yoshino, T., & Ito, E. (2010). Adiabatic temperature profile in the mantle. *Physics of the Earth and Planetary Interiors*, *183*(1–2), 212–218. https://doi.org/10.1016/j.pepi.2010.07.001

Khan, A., Huang, D., Durán, C., Sossi, P. A., Giardini, D., & Murakami, M. (2023). Evidence for a liquid silicate layer atop the Martian core. *Nature*, *622*(7984), 718–723. https://doi.org/10.1038/s41586-023-06586-4

Khan, A., Sossi, P. A., Liebske, C., Rivoldini, A., & Giardini, D. (2022). Geophysical and cosmochemical evidence for a volatile-rich Mars. *Earth and Planetary Science Letters*, *578*, 117330. https://doi.org/10.1016/j.epsl.2021.117330

Li, B. (2003). Compressional and shear wave velocities of ringwoodite γ-Mg_2SiO_4 to 12 GPa. *American Mineralogist*, *88*(8–9), 1312–1317. https://doi.org/10.2138/am-2003-8-913

Liu, Q., Liu, W., Whitaker, M. L., Wang, L., & Li, B. (2008). Compressional and shear wave velocities of Fe_2SiO_4 spinel at high pressure and high temperature. *High Pressure Research*, *28*(3), 405–413. https://doi.org/10.1080/08957950802296287

Liu, X., Xiong, Z., Chang, L., He, Q., Wang, F., Shieh, S. R., et al. (2016). Anhydrous ringwoodites in the mantle transition zone: Their bulk modulus, solid solution behavior, compositional variation, and sound velocity feature. *Solid Earth Sciences*, *1*(1), 28–47. https://doi.org/10.1016/j.sesci.2015.09.001

Lognonné, P., Banerdt, W. B., Clinton, J., Garcia, R. F., Giardini, D., Knapmeyer-Endrun, B., et al. (2023). Mars seismology. *Annual Review of Earth and Planetary Sciences*, *51*(1), 643–670. https://doi.org/10.1146/annurev-earth-031621-073318

Lognonné, P., Banerdt, W. B., Giardini, D., Pike, W. T., Christensen, U., Laudet, P., et al. (2019). Seis: Insight's seismic experiment for internal structure of Mars. *Space Science Reviews*, *215*, 1–170. https://doi.org/10.1007/s11214-018-0574-6

Mao, Z., Lin, J. F., Jacobsen, S. D., Duffy, T. S., Chang, Y. Y., Smyth, J. R., et al. (2012). Sound velocities of hydrous ringwoodite to 16 GPa and 673 K. *Earth and Planetary Science Letters*, *331*, 112–119. https://doi.org/10.1016/j.epsl.2012.03.001

Nestola, F., Ballaran, T. B., Koch-Müller, M., Balic-Zunic, T., Taran, M., Olsen, L., et al. (2010). New accurate compression data for γ-Fe2SiO4. *Physics of the Earth and Planetary Interiors*, *183*(3–4), 421–425. https://doi.org/10.1016/j.pepi.2010.09.007

Nishihara, Y., Takahashi, E., Matsukage, K. N., Iguchi, T., Nakayama, K., & Funakoshi, K. I. (2004). Thermal equation of state of $(Mg_{0.91}Fe_{0.09})_2SiO_4$ ringwoodite. *Physics of the Earth and Planetary Interiors*, *143*, 33–46. https://doi.org/10.1016/j.pepi.2003.02.001

Pearson, D. G., Brenker, F. E., Nestola, F., McNeill, J., Nasdala, L., Hutchison, M. T., et al. (2014). Hydrous mantle transition zone indicated by ringwoodite included within diamond. *Nature*, *507*(7491), 221–224. https://doi.org/10.1038/nature13080

Prescher, C., & Prakapenka, V. B. (2015). Dioptas: A program for reduction of two-dimensional X-ray diffraction data and data exploration. *High Pressure Research*, *35*(3), 223–230. https://doi.org/10.1080/08957959.2015.1059835

Rivers, M., Prakapenka, V. B., Kubo, A., Pullins, C., Holl, C. M., & Jacobsen, S. D. (2008). The COMPRES/GSECARS gas-loading system for diamond anvil cells at the Advanced Photon Source. *High Pressure Research*, *28*(3), 273–292. https://doi.org/10.1080/08957950802333593

Samuel, H., Drilleau, M., Rivoldini, A., Xu, Z., Huang, Q., Garcia, R. F., et al. (2023). Geophysical evidence for an enriched molten silicate layer above Mars's core. *Nature*, *622*(7984), 712–717. https://doi.org/10.1038/s41586-023-06601-8

Shibazaki, Y., Ohtani, E., Terasaki, H., Suzuki, A., & Funakoshi, K. I. (2009). Hydrogen partitioning between iron and ringwoodite: Implications for water transport into the Martian core. *Earth and Planetary Science Letters*, *287*(3–4), 463–470. https://doi.org/10.1016/j.epsl.2009.08.034

Sinogeikin, S. V., Katsura, T., & Bass, J. D. (1998). Sound velocities and elastic properties of Fe-bearing wadsleyite and ringwoodite. *Journal of Geophysical Research*, *103*(B9), 20819–20825. https://doi.org/10.1029/98JB01819

Smyth, J. R., Holl, C. M., Frost, D. J., Jacobsen, S. D., Langenhorst, F., & Mccammon, C. A. (2003). Structural systematics of hydrous ringwoodite and water in Earth's interior. *American Mineralogist*, *88*(10), 1402–1407. https://doi.org/10.2138/am-2003-1001

Sturhahn, W. (2000). CONUSS and PHOENIX: Evaluation of nuclear resonant scattering data. *Hyperfine Interactions*, *125*(1–4), 149–172. https://doi.org/10.1023/A:1012681503686

Taylor, G. J. (2013). The bulk composition of Mars. *Geochemistry*, *73*(4), 401–420. https://doi.org/10.1016/j.chemer.2013.09.006

Toellner, T. S. (2000). Monochromatization of synchrotron radiation for nuclear resonant scattering experiments. *Hyperfine Interactions*, *125*(1/4), 3–28. https://doi.org/10.1023/A:1012621317798

Wang, F. (2024). Thermoelastic properties of iron-rich ringwoodite and the deep mantle aerotherm of Mars [Dataset]. *Zenodo*. https://doi.org/10.5281/zenodo.10946271

Weidner, D. J., Sawamoto, H., Sasaki, S., & Kumazawa, M. (1984). Single-crystal elastic properties of the spinel phase of Mg_2SiO_4. *Journal of Geophysical Research*, *89*(B9), 7852–7860. https://doi.org/10.1029/JB089iB09p07852

Yamanaka, T. (1986). Crystal structures of Ni_2SiO_4 and Fe_2SiO_4 as a function of temperature and heating duration. *Physics and Chemistry of Minerals*, *13*(4), 227–232. https://doi.org/10.1007/BF00308273

Ye, Y., Brown, D. A., Smyth, J. R., Panero, W. R., Jacobsen, S. D., Chang, Y. Y., et al. (2012). Compressibility and thermal expansion of hydrous ringwoodite with 2.5 (3) wt% H_2O. *American Mineralogist*, *97*(4), 573–582. https://doi.org/10.2138/am.2012.4010

Zhang, D., Dera, P. K., Eng, P. J., Stubbs, J. E., Zhang, J. S., Prakapenka, V. B., & Rivers, M. L. (2017). High pressure single crystal diffraction at PX^2. *Journal of Visualized Experiments*, e54660. https://doi.org/10.3791/54660

Zhou, W. Y., Zhang, J. S., Huang, Q., Lai, X., Chen, B., Dera, P., & Schmandt, B. (2022). High pressure-temperature single-crystal elasticity of ringwoodite: Implications for detecting the 520 discontinuity and metastable ringwoodite at depths greater than 660 km. *Earth and Planetary Science Letters*, *579*, 117359. https://doi.org/10.1016/j.epsl.2021.117359

References From the Supporting Information

Jacobsen, S. D., Smyth, J. R., Spetzler, H., Holl, C. M., & Frost, D. J. (2004). Sound velocities and elastic constants of iron-bearing hydrous ringwoodite. *Physics of the Earth and Planetary Interiors*, *143*, 47–56. https://doi.org/10.1016/j.pepi.2003.07.019

Kleppe, A. K., Jephcoat, A. P., Smyth, J. R., & Frost, D. J. (2002). On protons, iron and the high-pressure behavior of ringwoodite. *Geophysical Research Letters*, *29*(21), 17-1–17-4. https://doi.org/10.1029/2002gl015276

Koch-Müller, M., Rhede, D., Schulz, R., & Wirth, R. (2009). Breakdown of hydrous ringwoodite to pyroxene and spinelloid at high P and T and oxidizing conditions. *Physics and Chemistry of Minerals*, *36*(6), 329–341. https://doi.org/10.1007/s00269-008-0281-z

Taran, M. N., Koch-Müller, M., Wirth, R., Abs-Wurmbach, I., Rhede, D., & Greshake, A. (2009). Spectroscopic studies of synthetic and natural ringwoodite, γ-$(Mg, Fe)_2SiO_4$. *Physics and Chemistry of Minerals*, *36*(4), 217–232. https://doi.org/10.1007/s00269-008-0271-1

Thomas, S. M., Jacobsen, S. D., Bina, C. R., Reichart, P., Moser, M., Hauri, E. H., et al. (2015). Quantification of water in hydrous ringwoodite. *Frontiers in Earth Science*, *2*, 38. https://doi.org/10.3389/feart.2014.00038

Thomson, A. R., Piltz, R. O., Crichton, W. A., Cerantola, V., Ezad, I. S., Dobson, D. P., et al. (2021). Incorporation of tetrahedral ferric iron into hydrous ringwoodite. *American Mineralogist*, *106*(6), 900–908. https://doi.org/10.2138/am-2021-7539

Sinogeikin, S. V., Bass, J. D., & Katsura, T. (2001). Single-crystal elasticity of γ-$(Mg0.91Fe_{0.09})_2SiO_4$ to high pressures and to high temperatures. *Geophysical Research Letters*, *28*(22), 4335–4338. https://doi.org/10.1029/2001GL013843

Sinogeikin, S. V., Bass, J. D., & Katsura, T. (2003). Single-crystal elasticity of ringwoodite to high pressures and high temperatures: Implications for 520 km seismic discontinuity. *Physics of the Earth and Planetary Interiors*, *136*(1–2), 41–66. https://doi.org/10.1016/S0031-9201(03)00022-0